Tunable geometric phase of Dirac fermions in a topological junction

Sang-Jun Choi, Sunghun Park,* and H.-S. Sim†
Department of Physics, Korea Advanced Institute of Science and Technology, Daejeon 305-701, Korea
(Received 14 September 2012; published 10 April 2013)

We predict a tunable and nonadiabatic Berry phase effect of Dirac fermions, which is an electronic analog of the Pancharatnam phase of polarized light. The Berry phase occurs as a scattering phase shift in a single scattering event of transmission or reflection of Dirac fermions at a junction with a spatially nonuniform mass gap, unveiling the topological aspects of scattering of chiral Dirac fermions. This geometric phase plays different roles in solids as compared with the Pancharatnam phase in optics. It provides a unique approach of detecting the Chern number of the insulator side in a metal-insulator junction of Dirac fermions, implying a different type of bulk-edge correspondence at the boundary between a metal and an insulator. This phase also modifies the quantization rule of Dirac fermions, suggesting geometric-phase devices with nontrivial charge and spin transport such as a topological waveguide and a topological transistor.

DOI: 10.1103/PhysRevB.87.165420 PACS number(s): 73.23.−b, 03.65.Vf, 72.80.Vp, 73.20.−r

I. INTRODUCTION

Polarized light acquires a geometric phase when it passes through a series of polarizers.[1] This phase, known as the Pancharatnam phase,[1–4] is a topological phenomenon of geometric origin in a Poincaré sphere, a graphical tool representing light polarization on its surface; see Fig. 1. This phase was useful for generalizing the quantum geometric phase, known as the Berry phase,[5,6] from an adiabatic cyclic evolution of quantum states to discontinuous or noncyclic changes[2,3,7] such as projective measurement. It has attracted much attention in optics and is used in various optical devices.[3]

Electron spin can be considered as a counterpart of light polarization. It acquires Berry phase along a closed trajectory on the Bloch sphere, the object equivalent to a Poincaré sphere.[8] This analogy may motivate us to search for the effects of electrons corresponding to the Pancharatnam phase of polarized light, as such analogies between electronics and optics have often led to finding new interesting phenomena. However, the electron analog of the Pancharatnam phase of light has not been studied.

On the other hand, electrons in graphene[9] and on a surface of topological insulators[10–12] behave as Dirac fermions (DFs). They have the interesting property of spin-momentum locking that their spin rotates following the change in direction of the spatial momentum; in graphene, the pseudospin representing sublattice states behaves as the spin. Massless DFs acquire the Berry phase of π in spatial motion along a closed trajectory on a plane, as the their spin rotates along a great circle on the Bloch sphere. This special value π causes topological phenomena[13–17] such as the half-integer quantum Hall effect and weak antilocalization. When DFs become massive, they can have the other possible values of Berry phase of spin $1/2$. The continuous values of Berry phase cause the modification of the known effects of Berry phase π.[18–20] They may also result in new interesting effects, together with unusual transport[17,21–24] of DFs.

In this work, we theoretically show that DFs acquire Berry phase as a scattering phase shift in a *single nonadiabatic scattering* event of reflection or transmission at a junction with mass gap. This phase is an electron version of Pancharatnam phase, and the junction provides a platform for studying Pancharatnam phase in solids, as the phase can be tuned to an arbitrary value by junction control. This phase causes interesting effects. It has the information of the Chern number of the insulator side of a metal-insulator junction of DFs. This implies a type of bulk-edge correspondence for the boundary between *a metal and an insulator*, which is different from the conventional version of the correspondence with gapless edge states between two insulators with different Chern numbers. The phase also modifies the quantization rule of DFs, suggesting *geometric-phase devices* with nontrivial charge and spin transport such as a topological waveguide and a topological transistor.

II. BERRY PHASE OF DIRAC FERMIONS IN A JUNCTION

For illustration, we consider DFs in a two-dimensional (2D) step junction (xy plane) in Fig. 1(b). Their Hamiltonian is $H = \hbar v_F(k_x\sigma_x + k_y\sigma_y) + V(x) + \Delta(x)\sigma_z$, where $(V(x),\Delta(x)) = (V_l,\Delta_l)$ for $x < 0$ and (V_r,Δ_r) for $x > 0$; a step junction is realized when the length scales over which $V(x)$ and $\Delta(x)$ spatially vary are shorter than the Fermi wavelength of the DFs. They have Fermi velocity v_F, charge e, and the locking $\vec{k}\cdot\vec{\sigma}$ of momentum $\vec{k} = (k_x,k_y)$ and Pauli spin operators $\sigma_{x,y,z}$. In experiments, the electrostatic potential $V(x)$ is tuned by gates, and the mass gap $\Delta(x)$ is created in topological insulators by magnetic doping[19,20,25,26] or a ferromagnetic insulator.[27,28]

Pancharatnam phase $\mathcal{P}_p$ equals the Berry phase along a *geodesic polygon* p on the parameter space,[2] $\mathcal{P}_p = i\oint_p d\vec{k}\cdot\langle\vec{k}|\nabla_{\vec{k}}|\vec{k}\rangle = -\Omega_p/2$, where Ω_p is the solid angle of p. We find that $\mathcal{P}_p$ appears in the scattering of an incoming plane wave $|I\rangle$ at the step junction. In Fig. 1(b), $|I\rangle$ is reflected to state $|R\rangle$ or transmitted to $|T\rangle$. $|i = I,R,T\rangle$ has spin χ_i and satisfies the wave continuity $|I\rangle + \alpha|R\rangle = \beta|T\rangle$ at the interface $x = 0$, equivalently, $\chi_I + \alpha\chi_R = \beta\chi_T$, with reflection (transmission) coefficient α (β). By using $\chi_{\bar{T}}$ ($\chi_{\bar{A}}$ being the spin state orthogonal to χ_A), we obtain the reflection phase (see Appendix A) as

$$\arg\alpha = \pi - \arg(\chi_I^\dagger\chi_R) + \mathcal{P}_{I\bar{T}R}, \quad \mathcal{P}_{I\bar{T}R} = -\frac{\Omega_{I\bar{T}R}}{2}, \qquad (1)$$

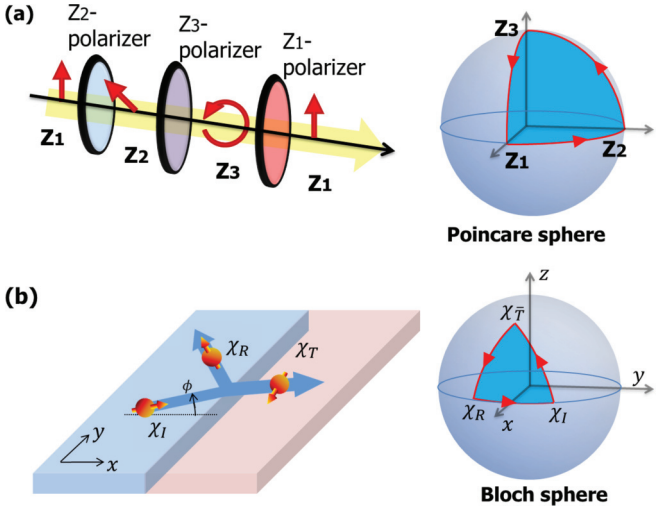

FIG. 1. (Color online) Pancharatnam phase of light and Dirac fermions. (a) Light with initial polarization Z_1 acquires Pancharatnam phase $-\Omega_{Z_1Z_2Z_3}/2$ after passing through polarizers with polarization axes Z_2, Z_3, and Z_1. (b) Dirac fermions acquire Pancharatnam phase $\mathcal{P}_{I\bar{T}R} = -\Omega_{I\bar{T}R}/2$ in a scattering event at a 2D step junction with mass gap. χ_I, χ_R, χ_T, and $\chi_{\bar{T}}$ denote the spin states involved in the scattering. Ω_{ABC} is the solid angle of the geodesic polygon on the Poincaré (Bloch) sphere which sequentially connects the vertices representing polarization (spin) states A, B, C (see arrows).

where $\chi_i^\dagger \chi_j$ denotes the inner product of spin states. In addition to the shift π by reflection and the gauge-dependent term of $\arg(\chi_I^\dagger \chi_R)$, $\arg\alpha$ has Berry phase $\mathcal{P}_{p=I\bar{T}R}$, which can be considered as a Pancharatnam phase whose geodesic polygon $p = I\bar{T}R$ connects χ_I, $\chi_{\bar{T}}$, χ_R on the Bloch sphere and has a solid angle $\Omega_{I\bar{T}R}$. Similarly, another Pancharatnam phase $\mathcal{P}_{I\bar{R}T}$ contributes to the transmission phase as

$$\arg\beta = -\arg(\chi_I^\dagger \chi_T) + \mathcal{P}_{I\bar{R}T}, \quad \mathcal{P}_{I\bar{R}T} = -\frac{\Omega_{I\bar{R}T}}{2}. \tag{2}$$

The relations (1) and (2) reveal that the scattering, a noncyclic and discontinuous event "projectively measuring" spin, has geometric nature. $\mathcal{P}_p$ is gauge invariant and hence, physically observable. For example, one observes $\mathcal{P}_{I\bar{T}R}$ by measuring $\arg\alpha$, with tuning $|T\rangle$ but keeping $\arg(\chi_I^\dagger \chi_R)$ unchanged. As discussed later, one can also observe it by studying resonances of DFs, since it modifies the quantization rule of DFs. Contrary to usual Berry phases of spin 1/2 in solids, $\mathcal{P}_p$ is acquired by a *single* scattering event of DFs and is experimentally *tunable* to arbitrary values $\in (0,2\pi)$. Also, Ω_p provides an intuitive graphical understanding of $\mathcal{P}_p$. When DFs are massless everywhere [i.e., $\Delta(x) = 0$], $\mathcal{P}_p = 0$ or π.

The above findings change only quantitatively in a smooth junction where $V(x)$ and $\Delta(x)$ spatially vary smoothly around $x = 0$. In this case, the scattering of DFs at the junction and the resulting spin rotation become more adiabatic; hence, $\mathcal{P}_p$ is not necessarily obtained from a geodesic polygon but from a closed path following the spin rotation on the Bloch sphere. Note that $\mathcal{P}_p$ is considered as Pancharatnam phase only when p is a geodesic polygon. Except for this, our findings about $\mathcal{P}_p$ are common for both a smooth junction and a step junction.

III. BULK-EDGE CORRESPONDENCE BY GEOMETRIC PHASE

$\mathcal{P}_p$ plays significant roles in solids, which are different from those of the Pancharatnam phase in optics. For example, $\mathcal{P}_p$ can be used for detecting the Chern number[29] that characterizes the topological order of a DF insulator with mass gap.

To see this, we consider a metal-insulator step junction with $\Delta_l = 0$ and $\Delta_r \neq 0$. The Chern number $\mathcal{C}$ of the insulator is related to the energy-gap parameter Δ_r of the insulator as $\mathcal{C} = -[1 + \mathrm{sgn}(\Delta_r)]/2$. In this case, a plane wave $|I\rangle$, propagating from the metal l to insulator r with incidence angle ϕ, is reflected to $|R\rangle$ via an evanescent state $|E\rangle$ of the insulator; its energy ϵ is inside the gap Δ_r, and $\phi = 0$ at normal incidence. Then, one finds that $\mathcal{P}_{p=I\bar{E}R}$ appears in the reflection phase $\arg\alpha$ of the wave, $\arg\alpha = \pi - \arg(\chi_I^\dagger \chi_R) + \mathcal{P}_{I\bar{E}R}$, where $|E\rangle$ replaces $|T\rangle$ in Eq. (1) and Fig. 1.

We show that the Chern number $\mathcal{C}$ of the insulator is identified by $\mathcal{P}_{I\bar{E}R}$. In Fig. 2(a) we find the topological property that the direction of the spin χ_E of $|E\rangle$ depends on $\mathcal{C}$. For any $|E\rangle$, the xy component of χ_E aligns parallel (antiparallel) to the junction interface when $\mathcal{C} = -1$ ($\mathcal{C} = 0$). Namely, $\mathcal{C}$ represents the winding number of χ_E along insulator edges. This property is recognized by $\mathcal{P}_{I\bar{E}R}$. For example, for $\phi = 0^{\pm}$, $0^{+(-)}$ being positive (negative) infinitesimal, we find (see Appendix B) that $\mathcal{P}_{I\bar{E}R}$ covers different domains for different $\mathcal{C}$ [see Fig. 2(b)]:

$$\mathcal{C} < s_\phi \cos\mathcal{P}_{I\bar{E}R}(\epsilon, \phi = 0^{\pm}) < 1 + \mathcal{C}. \tag{3}$$

The sign factor $s_\phi = \mathrm{sgn}[\sin(2\phi)]$ results from the intrinsic property[30] of Pancharatnam phase that $\mathcal{P}_{I\bar{E}R}$ jumps by Berry phase π at $\phi = 0$. For $\phi \neq 0$, $\mathcal{P}_{I\bar{E}R}$ also recognizes $\mathcal{C}$

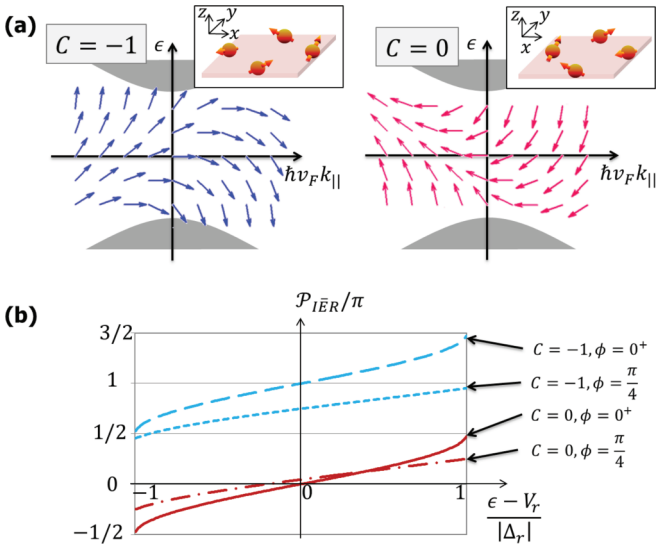

FIG. 2. (Color online) Spin of evanescent states and Chern number. (a) Spin direction (arrows) of evanescent states in an edge of an insulator (xy plane), whose energy and momentum tangential to the edge are denoted as ϵ and $k_\parallel$, respectively; its xy (z) component is drawn parallel to the $k_\parallel$ (ϵ) axis and depends on the Chern number $\mathcal{C}$ of the insulator energy band (shade). When $\mathcal{C} = -1$ ($\mathcal{C} = 0$), the xy spin component aligns parallel (antiparallel) to the edge (see the insets). (b) Pancharatnam phase $\mathcal{P}_{I\bar{E}R}(\epsilon)$ for different $\mathcal{C}$ and ϕ. It detects the spin alignment. At $\phi = 0^+$, $\mathcal{P}_{I\bar{E}R}(\epsilon)$ covers different domains for different $\mathcal{C}$, regardless of junction details.

via another inequality (see Appendix C). We remark that inequality (3) is independent of the junction details of ϵ, $V_{l,r}$, and $|\Delta_{l,r}|$.

This finding shows a different version of bulk-edge correspondence for Z_2 insulators of DFs, $\mathcal{P}_{l\bar{E}R}$, a geometric phase occurring at a *metal-insulator* junction, recognizing $\mathcal{C}$, another geometric phase characterizing the energy-band topology of the insulator side. It is interesting to compare this with the conventional version of bulk-edge correspondence,[29] which states gapless metallic edge states in a junction of *two insulators* with different Chern numbers. We will discuss later the equivalence between the two versions.

There are implications from the above. First, the existence of $\mathcal{P}_p$ in a metal-insulator junction is related to the bulk-edge correspondence and hence may be topologically guaranteed, regardless of junction details [such as the spatial dependence of $V(x)$ and $\Delta(x)$]. Second, a similar bulk-edge correspondence may also exist for general metal-insulator junctions of non-DFs. For example, one considers the situation that two-dimensional electrons form a junction of a metal and a quantum Hall insulator, where an external magnetic field is applied only to the quantum Hall region, and focuses on the scattering phase shift of an electron plane wave incoming from the metal and reflected by the insulator. The phase shift is caused by the phase accumulation along the cyclotron motions, which form evanescent states in the insulator. This phase corresponds to the Pancharatnam phase of the DF case and has the information of the filling factor of the quantum Hall insulator.

IV. CONTRIBUTION OF GEOMETRIC PHASE TO QUANTIZATION

We discuss another property that $\mathcal{P}_p$ modifies the quantization rule. Equation (1) leads to the Bohr-Sommerfeld semiclassical rule for a closed trajectory with length d and $k = |\vec{k}|$,

$$kd + m_p\pi + \mathcal{P}_p = 2\pi n, \quad n = 0,1,2,\ldots, \tag{4}$$

which has dynamical phase kd and π shift at each of m_p reflections in the trajectory. $\mathcal{P}_p$ is the new contribution from the geodesic polygon p connecting the states (propagating χ_{k_j} or evanescent χ_{e_j}) involved along the trajectory in sequential order. For the bound state in Fig. 3(a), we find $p = k_1\bar{e}_1k_2\bar{e}_2k_3\bar{e}_3k_4\bar{e}_4$. The geometric contribution of $\mathcal{P}_p$ is obtained by adding up the reflection phases $\arg\alpha$ from the reflection events along the trajectory. It should be mentioned that all the terms, including the second gauge-dependent term of Eq. (1), contribute to $\mathcal{P}_p$, since the gauge-dependent terms occurring in the reflection events of a closed trajectory together constitute a geodesic polygon on the Bloch sphere, thus becoming gauge invariant. The geometric contribution $\mathcal{P}_p$ to the quantization rule can be detected by observing bound states with tuning χ_{e_j}'s, or from its unusual implications with regard to interference, resonance, and quantum transport.

As an example, we consider a *topological* waveguide g with width w, sandwiched between two insulators l,r with mass gaps Δ_l and Δ_r, and Chern numbers $\mathcal{C}_l$ and $\mathcal{C}_r$ [see Fig. 3(b)]. The waveguide has propagating states and is tuned by gate voltage V_g. The quantization rule for the waveguide

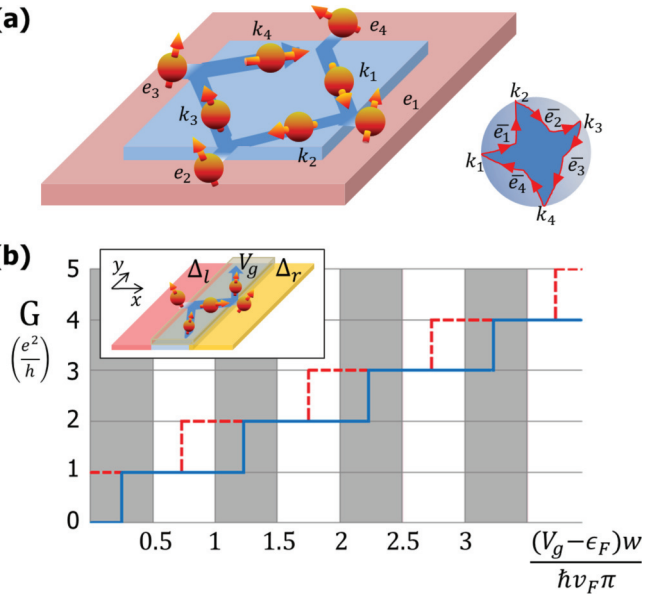

FIG. 3. (Color online) Contribution of Pancharatnam phase to quantization. (a) A bound trajectory in a metallic box surrounded by insulators. Its quantization is affected by Pancharatnam phase from the geodesic polygon (see Bloch sphere) connecting the scattering states (k_j,e_j) involved along the trajectory. (b) Electron conductance $G(V_g)$ along a topological waveguide g with width w, sandwiched between two insulators $j = l,r$ with band gap $\Delta_{j=l,r}$ and Chern number $\mathcal{C}_{j=l,r}$; ϵ_F is inside the gaps $\Delta_{j=l,r}$. Inside the guide g, gate voltage V_g is applied and there is no gap ($\Delta_g = 0$). For $\mathcal{C}_l = \mathcal{C}_r$ ($\mathcal{C}_l \neq \mathcal{C}_r$), conductance jumps by e^2/h appear only within the shaded (white) domains of V_g. The examples of $G(V_g)$ are drawn for the cases of $\mathcal{C}_l = \mathcal{C}_r$ (blue solid line) and $\mathcal{C}_l \neq \mathcal{C}_r$ (red dashed).

states is

$$2k_xw + \mathcal{P}_{A\bar{E}_lB\bar{E}_r} = 2\pi n, \tag{5}$$

where $\mathcal{P}_{A\bar{E}_lB\bar{E}_r} = \mathcal{P}_{A\bar{E}_lB} + \mathcal{P}_{B\bar{E}_rA}$. $\mathcal{P}_{A\bar{E}_lB}$ occurs in the reflection from state A of momentum $(-k_x,k_y)$ in waveguide g to the state B of momentum (k_x,k_y) via an evanescent state $|E_l\rangle$ of insulator l, while $\mathcal{P}_{B\bar{E}_rA}$ from B to A via an evanescent state $|E_r\rangle$ of insulator r. Contrary to usual nontopological cases without $\mathcal{P}_p$, the quantization rule in Eq. (5) depends on k_y, as $\mathcal{P}_{A\bar{E}_lB\bar{E}_r}$ is a function of k_y. Electron conductance $G(V_g)$ along the waveguide g jumps by e^2/h as V_g varies whenever an additional channel satisfies Eq. (5).

When $w \to 0$, Eq. (5) becomes $\mathcal{P}_{A\bar{E}_lB} + \mathcal{P}_{B\bar{E}_rA} = 0$, namely, $\chi_{E_l} = \chi_{E_r}$. Its solution exists when $\mathcal{C}_l \neq \mathcal{C}_r$, describing edge states along the interface between insulators l and r. However, it never exists when $\mathcal{C}_l = \mathcal{C}_r$; one can see this by analyzing $\Omega_{A\bar{E}_lB\bar{E}_r}$. Hence, our bulk-edge correspondence based on $\mathcal{P}_p$ leads to the conventional version[29] based on edge states. The converse may be also true. The conventional version indicates that the waveguide with $\mathcal{C}_l \neq \mathcal{C}_r$ has more states than that of $\mathcal{C}_l = \mathcal{C}_r$. This implies the existence of the correspondence for a metal-insulator junction that the right half of the whole system, which is the junction of metal g and insulator r, has some dependence on $\mathcal{C}_r$ such as Eq. (3).

When w is finite, the waveguide shows another topological feature of $G(V_g)$ [see Fig. 3(b)]. When its Fermi energy ϵ_F satisfies $\epsilon_F(V_g - \epsilon_F) \leqslant 0$, the jumps of $G(V_g)$ by e^2/h

occur within the domains of V_g that have no overlap between the cases of $\mathcal{C}_l = \mathcal{C}_r$ and $\mathcal{C}_l \neq \mathcal{C}_r$. The jumps occur within the domains of $|V_g - \epsilon_F|w/(\pi\hbar v_F) \in (n, n+0.5)$ for $\mathcal{C}_l = \mathcal{C}_r$, while $|V_g - \epsilon_F|w/(\pi\hbar v_F) \in (n+0.5, n+1)$ for $\mathcal{C}_l \neq \mathcal{C}_r$; $n = 0,1,2,\ldots$. The origin is that the winding direction of $p = A\bar{E}_l B\bar{E}_r$ is opposite between the two cases (see Appendix D). Hence, the topologically different cases of $\mathcal{C}_l = \mathcal{C}_r$ and $\mathcal{C}_l \neq \mathcal{C}_r$ are distinguished by the conductance jumps. This feature is useful for detecting $\mathcal{P}_p$.

V. GEOMETRIC-PHASE DEVICE

The above features of $\mathcal{P}_p$ suggest geometric-phase devices with new functionality. In Fig. 4 we consider a Fabry-Pérot resonator; it has the same setup as the waveguide, but Fermi energy ϵ_F is located above the gaps $\Delta_{l,r}$. The transmission probability of a plane wave through the resonator is well known but modified by the quantization rule in Eq. (5) as

$$\tau = \frac{|\beta_l \beta_r|^2}{1 + |\alpha_l \alpha_r|^2 - 2|\alpha_l \alpha_r| \cos\left(2k_x w + \mathcal{P}_{A\bar{E}_l B\bar{E}_r}\right)}, \tag{6}$$

where $|\alpha_{i=l,r}|^2$ ($|\beta_i|^2$) is the reflection (transmission) probability at the interface between regions i and g, and $|E_i\rangle$ now means the propagating state of region i. Note that Fabry-Pérot resonators of DFs have been studied in different contexts from $\mathcal{P}_p$ in literature.[21,22,31]

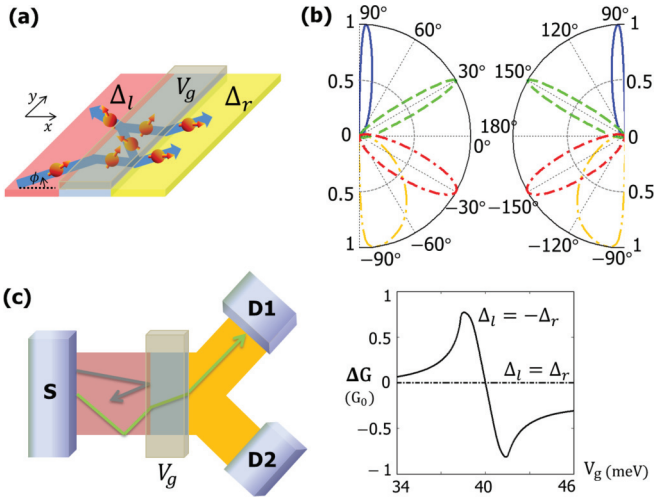

FIG. 4. (Color online) Geometric-phase device. (a) Topological Fabry-Pérot resonator, consisting of three regions $j = l,g,r$ with gap $\Delta_{j=l,r}$ and gate voltage $V_{j=l,g,r}$. (b) Transmission probability $\tau(\phi)$ of a plane wave, incoming from the left region l (see left panel) or right region r (right panel) with incidence angle ϕ, through the resonator with $\Delta_l = -\Delta_r$ and $V_l = V_r$. The results for different V_g are drawn by curves of different style. (c) Multiterminal field-effect transistor based on the resonator in a Y junction; region r now has two drains, D1 and D2, which are mirror-reflection symmetric. In the right panel, $\Delta G(V_g) \equiv (G_1(V_g) - G_2(V_g))/(G_1(V_g) + G_2(V_g))$ is drawn as a function of V_g at zero temperature in the zero-bias limit, where G_1 (G_2) is electron conductance from source S to D1 (D2). While $G_1 = G_2$ is always satisfied for $\Delta_1 = \Delta_2$, ΔG is generally nonzero for $\Delta_l = -\Delta_r$, although the setup has the mirror reflection symmetry. For the details of this figure, see Appendix E.

Figure 4(b) shows $\tau(\phi)$ for a plane wave with energy ϵ_F incoming from the left region l with incidence angle $\phi \in (-\pi/2, \pi/2)$ or from the right region r with $\phi \in (-\pi, -\pi/2) \cup (\pi/2, \pi)$. The plane wave can pass through the resonator only near the resonance angles of ϕ satisfying $2k_x w + \mathcal{P}_{A\bar{E}_l B\bar{E}_r} = 2n\pi$, which is controllable by V_g. Interestingly, the occurrence of the resonance is (more) asymmetric, $\tau(\phi) \neq \tau(-\phi)$ with respect to $\phi = 0$ for (larger) $\mathcal{P}_{A\bar{E}_l B\bar{E}_r} \neq 0$. And $\tau(\phi) \neq \tau(\phi + \pi)$, causing the possibility that when a state from region l resonantly passes through the resonator to a state $|E_r\rangle$ of region r, the time-reversed state of $|E_r\rangle$ cannot pass to l. This is because the two processes are affected by different $\mathcal{P}_{A\bar{E}_l B\bar{E}_r}$. Conventional resonators do not have these topological features.

In Fig. 4(c) we consider a multiterminal transistor based on the resonator and study electron conductance G_i from source S to drain i (D1 for $i = 1$ and D2 for $i = 2$). When $\Delta_l = \Delta_r$, $G_1 = G_2$ is always satisfied, since $\mathcal{P}_{A\bar{E}_l B\bar{E}_r} = 0$, and by tuning V_g, one switches on and off current to D1 and D2 simultaneously. In contrast, when $\Delta_l \neq \Delta_r$, $G_1 \neq G_2$ in general, since $\tau(\phi) \neq \tau(-\phi)$. Using V_g, one controls $\Delta G \propto (G_1 - G_2)/(G_1 + G_2)$, and switches on and off G_1 and G_2 separately. Moreover, since $\tau(\phi) \neq \tau(\phi + \pi)$, this device also behaves as a diode where current from S to D1 or D2 (from D1 or D2 to S) is switched on (off). This example demonstrates that combined with the unusual transport of DFs,[17,21–24] $\mathcal{P}_p$ will open a unique way to topological electronics, as it is acquired in local scattering of propagating DFs and tunable to arbitrary values.

VI. DISCUSSION

To summarize, DFs acquire Berry phase $\mathcal{P}_p$, an electronic analog of the Pancharatnam phase of polarized light, in a nonadiabatic scattering event at a junction with mass gap. It leads to a type of bulk-edge correspondence for a metal-insulator junction and this phase also contributes to the quantization rule of DFs and leads to geometric-phase devices.

We note that $\mathcal{P}_p$ will ubiquitously appear, with some modification, in various systems, including one-dimensional (1D) zigzag edges of graphene, nonplanar 2D surfaces,[32,33] bilayer graphene with mass gap, and photonic crystals.[34] For example, a plane wave of DFs acquires $\mathcal{P}_p$ in a scattering event by the zigzag edge while it does not in an armchair edge.[35] In nonplanar 2D surfaces, massless DFs can acquire $\mathcal{P}_p$ since their spin does not lie on a 2D plane. Bilayer graphene is of special interest, as the mass gap of its DFs is tuned by electrostatic gates.[36]

ACKNOWLEDGMENTS

We thank A. H. MacDonald and J. E. Moore for discussions, UC Berkeley, where part of this paper was written, for hospitality, and support from Korea NRF (Grant No. 2011-0022955).

APPENDIX A : DERIVATION OF EQS. (1) AND (2)

To derive Eq. (1), one starts with the continuity of the waves, $|I\rangle + \alpha|R\rangle = \beta|T\rangle$, at the junction interface $x = 0$.

It is rewritten as $\chi_I + \alpha\chi_R = \beta\chi_T$. By applying $\chi_{\bar{T}}^\dagger$ to this and using $\chi_{\bar{T}}^\dagger\chi_T = 0$, one finds $\alpha = -(\chi_{\bar{T}}^\dagger\chi_I)/(\chi_{\bar{T}}^\dagger\chi_R)$. Next, one uses the geodesic rule[2,37] of $\arg(\chi_a^\dagger\chi_b) = i\int_{b\to a} ds\,\chi_s^\dagger\nabla_s\chi_s$, where $s: b \to a$ is the geodesic line from χ_b to χ_a on the Bloch sphere. By combining the rule and $\mathcal{P}_{I\bar{T}R} \equiv \arg[(\chi_I^\dagger\chi_R)(\chi_R^\dagger\chi_{\bar{T}})(\chi_{\bar{T}}^\dagger\chi_I)]$, one obtains Eq. (1). In the same way, one can derive Eq. (2).

APENDIX B : TOPOLOGICAL PROPERTY OF χ_E IN FIG. 2

The dependence of χ_E on $\mathcal{C}$ is obtained as follows. χ_E is represented as $\chi_E^\dagger = (\cos\frac{\theta}{2}, -is\sin\frac{\theta}{2})$, with $s = \mathrm{sgn}(\Delta_r\kappa_x)$ and $\theta \in [0,\pi]$. Here κ_x comes from the purely imaginary momentum $k_x = i\kappa_x$ of $|E\rangle$ in $\hat{x}$ direction (toward the insulator), and it satisfies $\hbar v_F\kappa_x = [\Delta_r^2 + (\epsilon - V_l)^2\sin^2\phi - (\epsilon - V_r)^2]^{1/2}$; ϵ is the energy measured relative to the energy at $\vec{k} = 0$ of the insulator side, and θ satisfies $\tan\frac{\theta}{2} = |\frac{\hbar v_F\kappa_x + |\epsilon - V_l|\sin\phi}{\Delta_r + \epsilon - V_r}|$. The sign factor s of χ_E gives the property that the component of χ_E tangential to the insulator edge is parallel or antiparallel to the edge, depending on $\mathcal{C}$.

We note the details of Fig. 2(b). In the figure we choose $V_l = 0$ and $V_r = 0.5|\Delta_r|$, and ϵ is measured relative to the energy at $\vec{k} = 0$ of the metal.

APPENDIX C : DERIVATION OF INEQUALITY (3)

Here we derive the inequality (3). The case of $\phi = 0^\pm$ is useful for understanding $\mathcal{P}_{I\bar{E}R}$, as $\Omega_{I\bar{E}R}$ has simple dependence on $|E\rangle$. In this case, one finds the analytic expression of

$$\mathcal{P}_{I\bar{E}R}(\epsilon,\Delta_r,\phi = 0^\pm) = -\mathrm{sgn}(\Delta_r)\theta(\epsilon,\Delta_r) - s_\phi\pi/2,$$

where $s_\phi = \mathrm{sgn}[\sin(2\phi)]$. This leads to Eq. (3).

The first term of the above equation shows that $\mathcal{P}_{I\bar{E}R}$ is directly related to the angle θ of χ_E and $\mathrm{sgn}(\Delta_r)$. Because of the term $\mathrm{sgn}(\Delta_r)$, $\mathcal{P}_{I\bar{E}R}$ recognizes the topological order or $\mathcal{C}$. The dependence on θ and $\mathrm{sgn}(\Delta_r)$ results in the domain of the inequality (3). The second term of $s_\phi\pi/2$ is originated from the fact that when $\phi = 0$, $\mathcal{P}_{I\bar{E}R}$ is ill defined and jumps by π; notice that χ_I is orthogonal to χ_R and parallel to χ_T when $\phi = 0$. The π jump is the intrinsic topological property of $\mathcal{P}_p$ (Ref. 30) that the jump corresponds to Berry phase π by the 2π rotation of spin 1/2, equivalently, to the net solid angle 2π by $\mathcal{P}_{I\bar{E}R}(\phi = 0^+) - \mathcal{P}_{I\bar{E}R}(\phi = 0^-)$.

The inequality (3) is the case of the normal incidence of $\phi = 0^\pm$. We below provide another inequality for $\phi \neq 0$,

$$\mathcal{C} < s_\phi s_V \sin[\mathcal{P}_{I\bar{E}R}(\epsilon,-\phi) - \mathcal{P}_{I\bar{E}R}(\epsilon,\phi)] < 1 + \mathcal{C},$$

where $s_V = \mathrm{sgn}(V_r - V_l)$. This inequality shows that at finite $\phi \neq 0$, $\mathcal{P}_{I\bar{E}R}$ also recognizes $\mathcal{C}$, manifesting its asymmetric nature with respect to $\phi = 0$. This inequality is also independent of junction details as inequality (3). The derivation of this inequality requires some lengthy algebra of sinusoid functions, as no simple expression of $\mathcal{P}_{I\bar{E}R}$ for $\phi \neq 0$ is available. We do not provide the details of the derivation here. Instead, we mention that the asymmetric nature of $\mathcal{P}_{I\bar{E}R}$ with respect to $\phi = 0$ in the inequality originates from the dependence of the winding direction of the geodesic polygon $I\bar{E}R$ on $\mathrm{sgn}(\phi)$.

We mention about the case of $V_r = V_l$ in the above inequality. When $V_r = V_l$ and ϕ is finite, $\mathcal{P}_{I\bar{E}R}(\epsilon,-\phi) - \mathcal{P}_{I\bar{E}R}(\epsilon,\phi) = \pm\pi$; hence, $\sin[\mathcal{P}_{I\bar{E}R}(\epsilon,-\phi) - \mathcal{P}_{I\bar{E}R}(\epsilon,\phi)] = 0$.

APPENDIX D : DERIVATION OF THE TOPOLOGICAL PROPERTY AND DETAILS OF FIG. 3(b)

Figure 3(b) shows the topological property that for $\epsilon_F(V_g - \epsilon_F) \leqslant 0$ (i.e., for $\epsilon_F \geqslant 0, V_g$ or $\epsilon_F \leqslant 0, V_g$), the conductance jumps by e^2/h at the value $V_{g,n}$ of the gate voltage V_g,

$$\begin{aligned} &\frac{|V_{g,n} - \epsilon_F|w}{\pi\hbar v_F} \in (n, n + 0.5] \quad \text{for} \quad \mathcal{C}_l = \mathcal{C}_r, \\ &\frac{|V_{g,n} - \epsilon_F|w}{\pi\hbar v_F} \in (n + 0.5, n + 1] \quad \text{for} \quad \mathcal{C}_l \neq \mathcal{C}_r, \end{aligned} \tag{D1}$$

where $n = 0,1,2,\ldots$. The domains have no overlap between the two cases of $\mathcal{C}_l = \mathcal{C}_r$ and $\mathcal{C}_l \neq \mathcal{C}_r$.

We derive this property below. First, we find the relation between the energy dispersion of the waveguide in Fig. 3(b) and the winding direction of the geodesic polygon $p = A\bar{E}_lB\bar{E}_r$. The dispersion is $(\epsilon - V_g)^2 = (\hbar v_F)^2(k_y^2 + k_x^2)$, and $\mathcal{P}_{p=A\bar{E}_lB\bar{E}_r}$ is derived as

$$\begin{aligned} \tan(|k_x|w) &= -t\tan\left[\frac{1}{2}\mathcal{P}_{A\bar{E}_lB\bar{E}_r}(t,k_x,k_y)\right] \\ &= \frac{(S_l + S_r)\hbar v_F|k_x|}{(S_l - S_r)\hbar v_F k_y + (\epsilon - V_g)(1 - S_lS_r)}, \end{aligned} \tag{D2}$$

where ϵ is the energy of the waveguide states, $t = \mathrm{sgn}(\epsilon - V_g)$, $S_l = \hbar v_F(\kappa_l - k_y)/(\Delta_l + \epsilon)$, $S_r = \hbar v_F(\kappa_r + k_y)/(\Delta_r + \epsilon)$, and $\hbar v_F\kappa_{l,r} = [\Delta_{l,r}^2 + (\hbar v_F k_y)^2 - \epsilon^2]^{1/2}$. To see the relation between the dispersion and the winding direction of $p = A\bar{E}_lB\bar{E}_r$, we rewrite the dispersion, using Eq. (D2), as $(\epsilon - V_g)^2 = (\hbar v_F)^2\{k_y^2 + [(n\pi - t\mathcal{P}_{A\bar{E}_lB\bar{E}_r}/2)/w]^2\}$, where n is an integer. Then, for $t = \mathrm{sgn}(\epsilon - V_g) = -1$, one finds that $(\hbar v_F)^2[k_y^2 + (n\pi/w)^2] < (\epsilon - V_g)^2 < (\hbar v_F)^2\{k_y^2 + [(n + 0.5)\pi/w]^2\}$ in the case of $\mathcal{P}_p \in (0,\pi)$, while $(\hbar v_F)^2\{k_y^2 + [(n - 0.5)\pi/w]^2\} < (\epsilon - V_g)^2 < (\hbar v_F)^2[k_y^2 + (n\pi/w)^2]$ in the other case of $\mathcal{P}_p \in (-\pi,0)$. Similar inequalities are found for $t = 1$. This shows that the bottoms of the energy bands (at which the conductance jumps) appear in energy domains that have no overlap between the cases of $\mathcal{P}_p \in (0,\pi)$ and $\mathcal{P}_p \in (-\pi,0)$ with different winding directions of p.

Next, we connect the winding direction of $p = A\bar{E}_lB\bar{E}_r$ with the difference between Chern numbers $\mathcal{C}_l$ and $\mathcal{C}_r$. For $\epsilon(V_g - \epsilon) \leqslant 0$, we derive $\mathrm{sgn}[\mathcal{P}_{A\bar{E}_lB\bar{E}_r}(s,k_x,k_y^n)] = -t\,\mathrm{sgn}(\Delta_l\Delta_r)$, where k_y^n is the value at which the group velocity of $d\epsilon/(\hbar dk_y)$ is zero and the conductance jumps. This relation shows that the winding direction of $p = A\bar{E}_lB\bar{E}_r$ is opposite between the two cases of $\mathcal{C}_l = \mathcal{C}_r$ and $\mathcal{C}_l \neq \mathcal{C}_r$. Combining this relation and the energy dispersion discussed in the last paragraph, one can prove the property of the topologically distinct domains in Eq. (D1).

The above connection between the winding direction of $p = A\bar{E}_lB\bar{E}_r$ and the difference of $\mathcal{C}_l - \mathcal{C}_r$ [hence the property in Eq. (D1)] is not always valid when $\epsilon(V_g - \epsilon) > 0$. It is because $\mathcal{P}_{p=A\bar{E}_lB\bar{E}_r}$ depends not necessarily only on Δ_r and Δ_l (i.e., $\mathcal{C}_l$ and $\mathcal{C}_r$), but also on states A and B of the waveguide.

We remark that in Eq. (D1), the domain boundaries of $|V_{g,n} - \epsilon_F|w/(\pi\hbar v_F) = n$ and $|V_{g,n} - \epsilon_F|w/(\pi\hbar v_F) = n + 0.5$ occur at $\mathcal{P}_{p=A\bar{E}_l B\bar{E}_r} = 0$ and $\mathcal{P}_{p=A\bar{E}_l B\bar{E}_r} = \pi$ (equivalently, $-\pi$), respectively.

The curves in Fig. 3(b) are drawn with parameters of $|\Delta_l| = |\Delta_r| = 10$ meV, $\epsilon_F = -7.5$ meV, $w = 62.8$ nm, and $v_F = 5 \times 10^5$ m/s. The blue solid line is drawn for $\Delta_l = \Delta_r$, while the red dashed one is for $\Delta_l = -\Delta_r$. The overall features of Fig. 3(b) do not depend on the details of the parameters.

APPENDIX E : DETAILED INFORMATION OF FIGS. 4(b) AND 4(c)

Figure 4(b) is drawn with parameters of $\Delta_l = -\Delta_r = 50$ meV, $V_l = V_r = 0$, $v_F = 5 \times 10^5$ m/s, $\epsilon = 50.001$ meV, and $w = 200$ nm. Different values of V_g are selected as $V_g = 42.02$ [see $\tau(\phi)$ drawn by the blue solid curve in Fig. 4(b)], 42.15 (green dashed), 42.33 (red dashed-dot), and 42.37 (yellow dashed-dot-dot) in units of millielectronvolts. We note that the result in Fig. 4(b) satisfies $\tau(\phi) = \tau(\pi - \phi)$, which is valid only for the specific case of $\Delta_l = -\Delta_r$ and $V_l = V_r$. The overall features of Fig. 4(b) do not depend on the details of the parameters.

In the Y junction of Fig. 4(c), we consider electron flow from source S to drain D1 or D2. Conductance G_i from the source to the ith drain (D1 for $i = 1$ and D2 for $i = 2$) is obtained at zero temperature in the zero-bias limit as

$$G_i = G_0 \int_{-\pi/2}^{\pi/2} d\phi\, T_i(\phi) \cos\phi, \quad i = 1,2, \tag{E1}$$

where $G_0 = (e^2/h)(Wk/\pi)$, W is the lateral width of region l of the waveguide, and $k = \sqrt{\epsilon^2 - \Delta_l^2}/(\hbar v_F)$. $T_i(\phi)$ is the probability that an electron incoming from S with incident angle ϕ to the resonator moves to the ith drain. It can be approximately written as $T_i(\phi) \simeq \tau(\phi)p_i(\phi)$, where $\tau(\phi)$ is the transmission probability through the resonator and p_i is the probability with which an electron moves to the ith drain after passing through the resonator. We compute p_i in a semiclassical way, with the parameters used in the computation of Fig. 4(b). Although this computation is not exact, it is enough to demonstrate that the asymmetry property of $G_1 \neq G_2$ occurs and that the asymmetry measure $\Delta G = (G_1 - G_2)/(G_1 + G_2)$ can be controlled by the gate voltage V_g applied to the resonator.

*lngch4@kaist.ac.kr
†hssim@kaist.ac.kr

[1] S. Pancharatnam, Proc. Indian Acad. Sci. A **44**, 247 (1956).
[2] M. V. Berry, J. Mod. Opt. **34**, 1401 (1987).
[3] R. Bhandari, Phys. Rep. **281**, 1 (1997).
[4] Y. Ben-Aryeh, J. Opt. B **6**, R1 (2004).
[5] M. V. Berry, Proc. R. Soc. A **392**, 45 (1984).
[6] J. Anandan, Nature (London) **360**, 307 (1992).
[7] Y. Aharonov and J. Anandan, Phys. Rev. Lett. **58**, 1593 (1987).
[8] D. Xiao, M.-C. Chang, and Q. Niu, Rev. Mod. Phys. **82**, 1959 (2010).
[9] A. H. Castro Neto, F. Guinea, N. M. R. Peres, K. S. Novoselov, and A. K. Geim, Rev. Mod. Phys. **81**, 109 (2009).
[10] M. Z. Hasan and C. L. Kane, Rev. Mod. Phys. **82**, 3045 (2010).
[11] J. E. Moore, Nature (London) **464**, 194 (2010).
[12] X.-L. Qi and S.-C. Zhang, Rev. Mod. Phys. **83**, 1057 (2011).
[13] K. S. Novoselov, A. K. Geim, S. V. Morozov, D. Jiang, M. I. Katsnelson, I. V. Grigorieva, S. V. Dubonos, and A. A. Firsov, Nature (London) **438**, 197 (2005).
[14] Y. Zhang, Y.-W. Tan, H. L. Stormer, and P. Kim, Nature (London) **438**, 201 (2005).
[15] F. Wilczek, Nat. Phys. **5**, 614 (2009).
[16] V. I. Fal'ko, K. Kechedzhi, E. McCann, B. L. Altshuler, H. Suzuura, and T. Ando, Solid State Commun. **143**, 33 (2007).
[17] C. W. J. Beenakker, Rev. Mod. Phys. **80**, 1337 (2008).
[18] H.-Z. Lu, J. Shi, and S.-Q. Shen, Phys. Rev. Lett. **107**, 076801 (2011).
[19] M. Liu, J. Zhang, C.-Z. Chang, Z. Zhang, X. Feng, K. Li, K. He, L.-l. Wang, X. Chen, X. Dai, Z. Fang, Q.-K. Xue, X. Ma, and Y. Wang, Phys. Rev. Lett. **108**, 036805 (2012).
[20] A. A. Taskin, S. Sasaki, K. Segawa, and Y. Ando, Phys. Rev. Lett. **109**, 066803 (2012).
[21] M. I. Katsnelson, K. S. Novoselov, and A. K. Geim, Nat. Phys. **2**, 620 (2006).
[22] S. Park and H.-S. Sim, Phys. Rev. Lett. **103**, 196802 (2009).
[23] S. Park and H.-S. Sim, Phys. Rev. B **84**, 235432 (2011).
[24] V. V. Cheianov, V. Fal'ko, and B. L. Altshuler, Science **315**, 1252 (2007).
[25] Y. Chen, J.-H. Chu, J. G. Analytis, Z. K. Liu, K. Igarashi, H.-H. Kuo, X. L. Qi, S. K. Mo, R. G. Moore, D. H. Lu, M. Hashimoto, T. Sasagawa, S. C. Zhang, I. R. Fisher, Z. Hussain, and Z. X. Shen, Science **329**, 659 (2010).
[26] S.-Y. Xu *et al.*, Nat. Phys. **8**, 616 (2012).
[27] Y. Tanaka, T. Yokoyama, and N. Nagaosa, Phys. Rev. Lett. **103**, 107002 (2009).
[28] P. D. Ye, D. Weiss, R. R. Gerhardts, M. Seeger, K. von Klitzing, K. Eberl, and H. Nickel, Phys. Rev. Lett. **74**, 3013 (1995).
[29] X.-L. Qi, Y.-S. Wu, and S.-C. Zhang, Phys. Rev. B **74**, 045125 (2006).
[30] R. Bhandari, Phys. Lett. A **157**, 221 (1991).
[31] T. Yokoyama, Y. Tanaka, and N. Nagaosa, Phys. Rev. Lett. **102**, 166801 (2009).
[32] J. Seo, P. Roushan, H. Beidenkopf, Y. S. Hor, R. J. Cava, and Ali Yazdani, Nature (London) **466**, 343 (2010).
[33] J. P. Dahlhaus, C.-Y. Hou, A. R. Akhmerov, and C. W. J. Beenakker, Phys. Rev. B **82**, 085312 (2010).
[34] Z. Wang, Y. Chong, J. D. Joannopoulos, and M. Soljačić, Nature (London) **461**, 772 (2009).
[35] S.-J. Choi, S. Park, and H.-S. Sim (in preparation).
[36] T. Ohta, A. Bostwick, T. Seyller, K. Horn, and E. Rotenberg, Science **313**, 951 (2006).
[37] J. Samuel and R. Bhandari, Phys. Rev. Lett. **60**, 2339 (1988).